



The role of water content in rate dependence of tensile strength of a fine-grained sandstone

Xin Cai^{1,2} · Chuanqing Cheng¹ · Yuan Zhao¹ · Zilong Zhou^{1,2} · Shaofeng Wang^{1,2}

Received: 11 November 2021 / Revised: 2 January 2022 / Accepted: 7 January 2022 / Published online: 28 January 2022
© Wrocław University of Science and Technology 2022

Abstract

Rocks in nature are commonly in partially saturated conditions and exposed to dynamic loads. In this study, to explore the coupled effects of water content and loading rate, dynamic Brazilian disc experiments were conducted on Yunnan sandstone samples with four levels of water content (from air-dried to water-saturated) under various loading rates (from 100 to 600 GPa/s) using a split Hopkinson pressure bar. The test results show that for each water content, the dynamic tensile strength of sandstone is positively sensitive to loading rate. The rate dependence of tensile strength increases as the rise of water content. The change trends of tensile strength against water content depend on loading rate: as water content rises, the tensile strength displays the manner of “no change followed by fast drop” at loading rates of 10^{-4} and 100 GPa/s. However, when the loading rate is above 200 GPa/s, the tensile strength increases first and then declines. The turning point occurs at water content between 1.0 and 2.0%. These observations can be interpreted with the competition between water weakening and enhancing effects under different loading conditions.

Keywords Water content · SHPB · Brazilian disc test · Tensile strength · Loading rate · Rate dependence

1 Introduction

In civil and rock engineering practices, rock structures often suffer water erosion, probably due to rain, rivers, underground water and atmospheric vapor [1]. Ubiquitous water weakens rock strength and stiffness [2] and further results in many geological and engineering disasters, such as landslides [3], tunnel collapse [4], and surface subsidence in mine area [5]. In reality, rock materials commonly fail via tension since their tensile strength (TS) is much lower than their compressive strength [6, 7]. Therefore, it is necessary to deeply understand the effects of water on the TS of rock for the safety and stability of structures built in or on rock foundations.

A large number of studies relevant to the water-weakening effect on the TS of various rock types under quasi-static loading conditions have been carried out, such as granite [8], gypsum [9], limestone [10], marble [11], mudstone [12], sandstone [13, 14] and siltstone [12, 15]. However, apart from quasi-static loads, rock structures are also usually subjected to instantaneous disturbances probably coming from blasting, drilling or earthquakes [16, 17]. From the view of loading rate (or strain rate), the deformation and fracture of rock exposed to these loading forms pertain to the dynamic category [18, 19]. Previous studies suggested that the mechanical responses of rocks under dynamic loading conditions vastly differ from those under quasi-static conditions [20, 21]. Considerable effort should also be made to explore the influence of water on the dynamic TS of rocks.

Research on the effects of water on the dynamic tensile behavior of rocks is less documented. In limited publications (e.g., [22, 23]), high loading rate experiments are only conducted under completely dry and water-saturated states. Nevertheless, for most in situ conditions, rocks are not in the two ultimate moisture states but in the intermediate-saturated state (varying water contents) [24, 25]. To date, the tensile behavior of rocks considering the coupled effects of dynamic loading and water content is still not reported.

✉ Yuan Zhao
zhaoyuan92@csu.edu.cn

Xin Cai
xincai@csu.edu.cn

¹ School of Resources and Safety Engineering, Central South University, Changsha 410010, Hunan, China

² Hunan Provincial Key Laboratory of Resources Exploitation and Hazard Control for Deep Metal Mines, Changsha 410010, Hunan, China

This paper aims to experimentally explore the influence of water content on the dynamic tensile behavior of sandstone. Four groups of sandstone samples with different water contents are prepared. Dynamic tests are performed on Brazilian disc sandstone samples under various loading rates using a split Hopkinson pressure bar. The dynamic TS of sandstone samples with different water contents is obtained and compared at specific loading rates. The changes in the rate dependence of TS against water content are revealed. The mechanisms of water effects on the dynamic TS of rock are elucidated. A brief review of important outcomes of pertinent prior works is exhibited in the next three subsections, followed by the test methodology. Subsequently, the test results and interpretations are presented.

2 Literature review

2.1 Testing methods for measuring tensile strength of rock-like materials

Due to the brittleness of rock-like materials, it is very difficult to accurately measure their TS. To date, several methods have been suggested [26, 27] to determine the TS of rock under quasi-static conditions, which can be generally categorized into two types: direct tension and indirect tension (including Brazilian disc (BD), flattened BD, Brazilian ring, three- or four-point bending, etc.). These methods can be extended to the dynamic loading region. Additionally, other dynamic indirect tensile methods have been proposed, such as dynamic semi-circular bending [28] and spalling tests [29].

The application of direct tension is very limited for rock materials because of its striking inherent disadvantages, such as complex sample geometry, high risk of misalignment and negligible stress concentration. For the indirect tension method, the BD test is currently the most widely used method due to the convenience for sample manufacturing and testing. Hence, it has been recommended by the International Society for Rock Mechanics and Rock Engineering (ISRM) as the standard method for obtaining rock TS under both quasi-static [30] and dynamic [31] loading conditions.

2.2 Water-weakening effects on the quasi-static tensile strength of rocks

Research on the water-weakening effects on the TS of rocks is much less documented compared to that on the uniaxial compressive strength [2]. For instance, Ojo and Brook [13] measured the TS of Woodkirk sandstone using direct tension tests. They reported that the TS of the sandstone is decreased by 50% from dry to water-saturated condition. They also found that the direct TS gradually recovers

with the evaporation of water in the rock sample. Vutukuri [10] conducted Brazilian ring tests on Indiana limestone immersed in water as well as other liquids. They suggested that the TS of limestone decreases exponentially with the dielectric constant and surface tension of the saturating liquids. Hashiba and Fukui [8] performed direct tension tests on four kinds of Japanese igneous rocks under dry and water-saturated conditions. They pointed out that the loss percentages of Japanese rocks after water saturation range from 7.6 to 58%. The water-induced reduction rate (ratio of dry strength to saturated strength) of TS is almost constant for different rocks, which is 1.61 greater times than that of UCS. Zhao et al. [14] explored the influence of water saturation on the TS of a low clay-bearing sandstone using BD tests. They discovered that the TS of sandstone is reduced by 41.3% after immersion for 16 days. However, the TS of the sandstone no longer drops as the immersion duration increases. Similar results were also observed on gypsum samples [9]. Erguler and Ulusay [12] qualified the influence of water content on the TS of 17 kinds of Turkish clay-bearing rocks. They stated that the TS reduction of rock is up to 90% with increasing water content. They also concluded that the TS of rocks has a negative exponential correlation with water content.

Figure 1 graphically illustrates the water-induced reduction in the quasi-static TS of different rock types. It is universally shared that water plays a weakening role in the TS of rocks under quasi-static condition, although there are remarkable differences in rock types, testing methods and loading environments. The TS loss induced by water saturation is primarily dependent on rock type. Moreover,

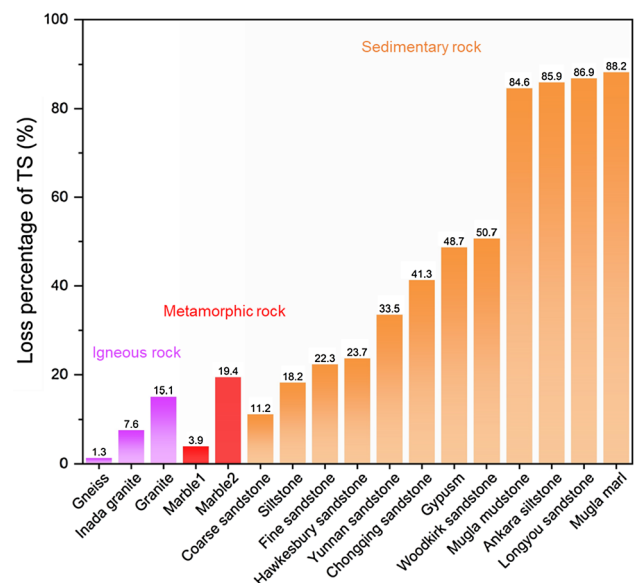


Fig. 1 Water-induced loss percentage for the TS of rocks under quasi-static condition. Data from [9, 10, 12, 14, 16, 17, 28, 31]

sedimentary rocks commonly experience higher TS loss than igneous and metamorphic rocks.

2.3 Effects of water on dynamic tensile strength and rate dependence of rock-like materials

With the development of rock dynamic testing techniques, research on the water effect on the dynamic TS of rocks has drawn attention in recent years [34]. For example, Ogata et al. [35] performed spalling tests on three Japanese rocks under dry and water-saturated conditions using a split Hopkinson pressure bar. They reported that water saturation lowers the dynamic TS of rocks with higher porosity (Kimachi sandstone and Tage tuff) but enhances their rate dependence. However, no significant variation is recognized in the dynamic TS of tight Inada granite with a low porosity of 0.49%. Cadoni [36] and Rossi [37] obtained the dynamic direct TS of concrete in different humidity environments and found that the dynamic TS of concrete rises as the relative humidity of testing condition increases at the same strain rate. They attributed this phenomenon to the Stefan effect and local damage reduction. Huang et al. [22] measured the

dynamic TS of dry and saturated sandstone samples using the dynamic BD method. They revealed that the reduction percentage of TS declines with increasing loading rate. Similar experiments were carried out on coal [38] and limestone [39] samples.

Figure 2 shows the relationship between the TS of rock-like materials and loading rates under dry and water-saturated conditions. The TS of both dry and saturated samples displays rate dependence. The TS is more sensitive to loading rate in saturated condition. In several studies [38, 39], the dynamic TS of saturated samples even exceeds that of dry samples.

3 Experimental methodology

3.1 Rock material and sample preparation

A sandstone with ideal homogeneity and isotropy obtained from Kunming, Yunnan (YN) province, China (called YN sandstone) is chosen as the testing material. The polarized image of thin section (Fig. 3a) shows that the YN sandstone

Fig. 2 Variations in the TS of dry and saturated samples against loading rate (hollow and solid symbols denote tested data of dry and saturated samples; dashed and continuous lines represent fitted lines for the data of dry and saturated samples). Data from [28, 32, 33, 47]

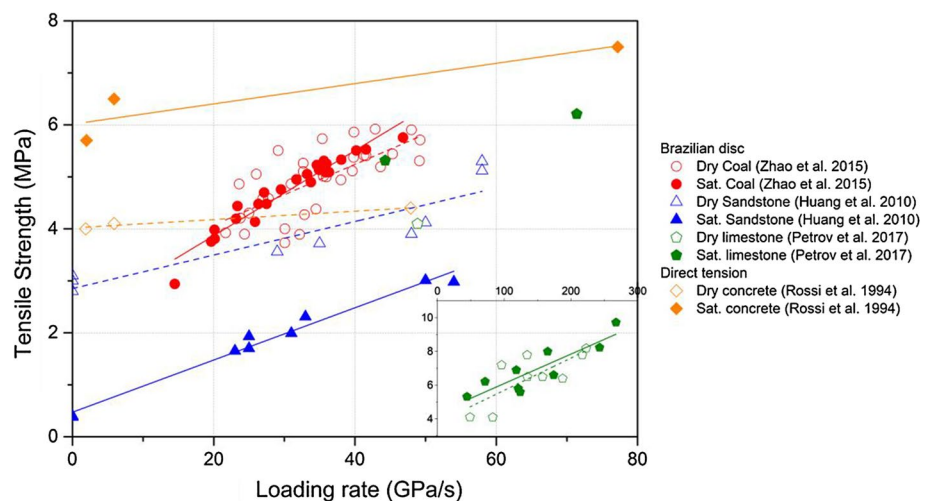
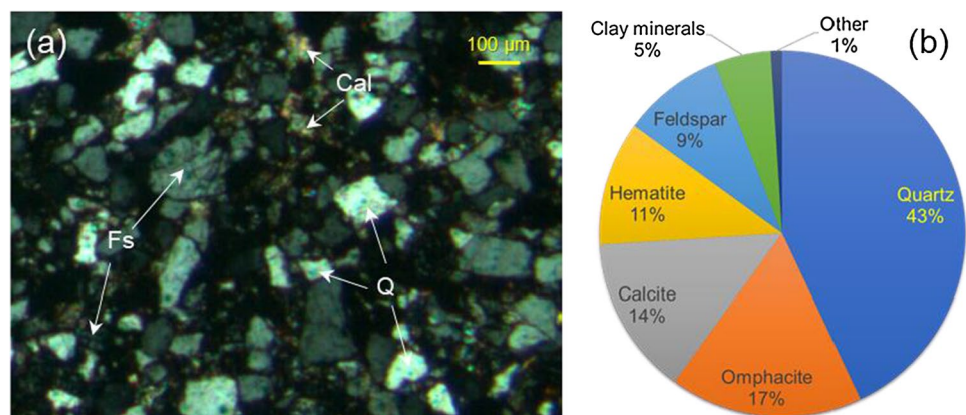


Fig. 3 **a** Microphotograph taken with a crossed polarizer and **b** mineral composition of the YN sandstone (*Q* quartz, *Cal* calcite, *Fs* feldspar)



is very tight without visible fractures and is fine-grained with an average grain size of 110 μm . Its grains are well cemented by calcite. According to energy dispersive X-ray analysis, the YN sandstone consists of 43% quartz, 17% omphacite, 14% calcite, 11% hematite, 9% feldspar, 5% clay minerals (mainly smectite) and 1% other minor minerals (see Fig. 3b). The average UCS of the YN sandstone is 60 MPa. The porosity of the YN sandstone obtained by water imbibition is $9.3 \pm 1.4\%$, which is very close to the value of $8.9 \pm 0.7\%$ measured by nuclear magnetic resonance (NMR). The YN sandstone has an average density of 2380 kg m^{-3} and a longitudinal wave speed of 2810 m s^{-1} .

All samples were obtained from the same sandstone slab without visible fractures to minimize the dispersion of sample properties [40]. Rock cylinders with a 50 mm diameter were cored from the sandstone slab. The cylindrical cores were then sliced into Brazilian discs with a length of 50 mm. All ends of each sample were carefully ground to make them parallel to each other. After that, all samples were placed in a laboratory with good ventilation for air-drying.

To obtain the relationship between water content and soaking duration, the mass of samples under dry condition was measured, and then the rock samples were submerged in distilled water for free soaking (Fig. 4a). The water content of rock sample is defined as

$$w = \frac{m_w - m_d}{m_d} \times 100\%, \quad (1)$$

where w is the water content of the sample; m_w and m_d are the masses of wet and dried samples.

Figure 4a shows the variation in water content in the YN sandstone sample via free soaking. The water content in the YN sandstone sample experiences three phases: fast

rising-slow rising-constant. After 24 h, the water content of the sandstone sample remains at 3.5%, indicating that the sample becomes completely water saturated. We considered that the maximum water absorption was approximately 3.5%. The water contents for testing were chosen at 0, 1.0, 2.0 and 3.5%, and the corresponding soaking time needed was 10 min, 30 min, 3 h and 24 h, respectively. We can obtain sandstone samples with the target water content accordingly.

3.2 Experimental setup

Dynamic BD tests were performed using a split Hopkinson pressure bar (SHPB) system placed at the Rock Impact Laboratory in School of Resources and Safety Engineering, Central South University. As shown in Fig. 5, the SHPB system includes a triggering unit, three central-aligned bars with a diameter of 50 mm (i.e., incident, transmitted and absorption bars), a data acquisition system (including an oscilloscope and a dynamic strain meter) and a high-speed photography system (including a high-intensity spotlight and a high-speed camera). The striker and three bars are made of high-strength alloy steel (40 Cr) with a density of 7800 kg m^{-3} , a yield strength of 725 MPa and an elastic modulus of 233 GPa. To eliminate the dispersion effect and achieve dynamic force equilibrium, we used the cone-shaped striker proposed by Li et al. [41] to generate the half-sine wave with a slow-rising edge (Fig. 6a). A more detailed introduction to the SHPB system can be found in previous publications [42, 43].

In SHPB tests, the dynamic force on both ends of the rock sample can be calculated as [21, 31]

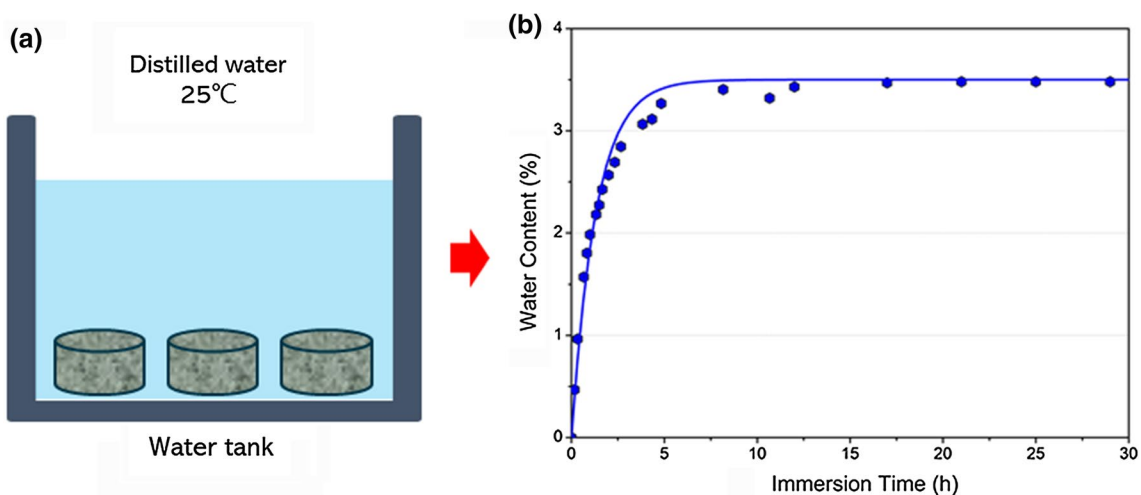


Fig. 4 a Illustration of free-soaking and b change in water content of the YN sandstone sample with immersion time

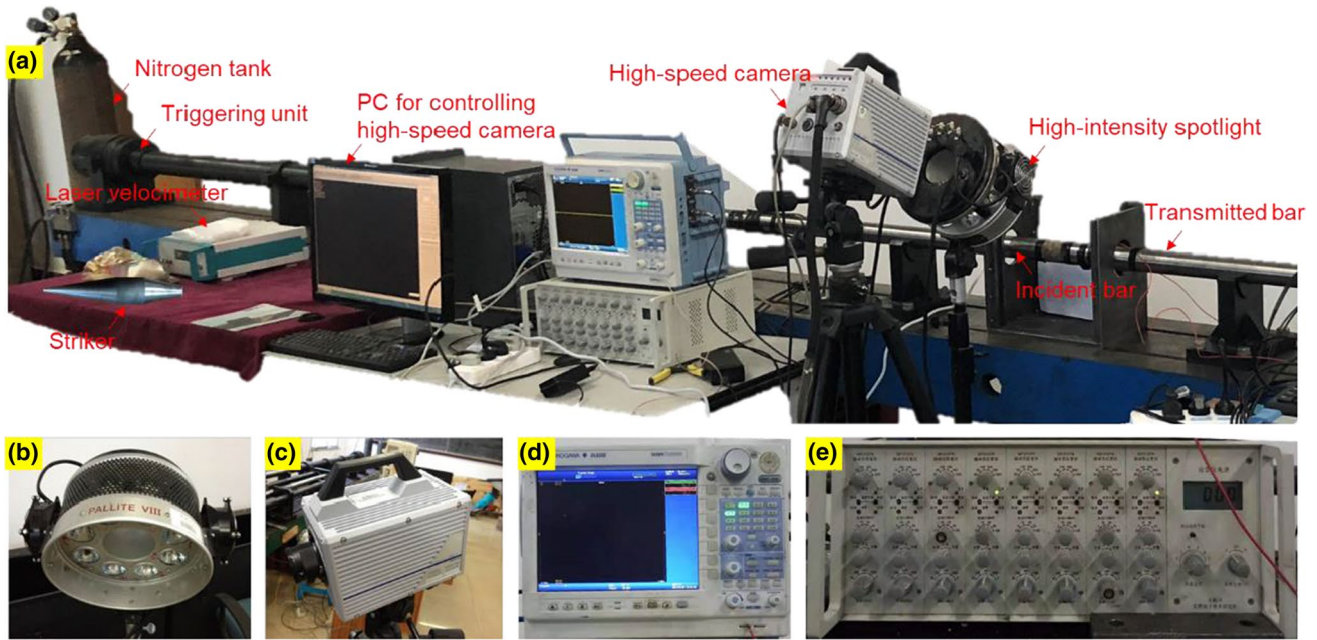


Fig. 5 a Overview of the SHPB system; b high-intensity spotlight; c high-speed camera; d oscilloscope; e dynamic strain meter

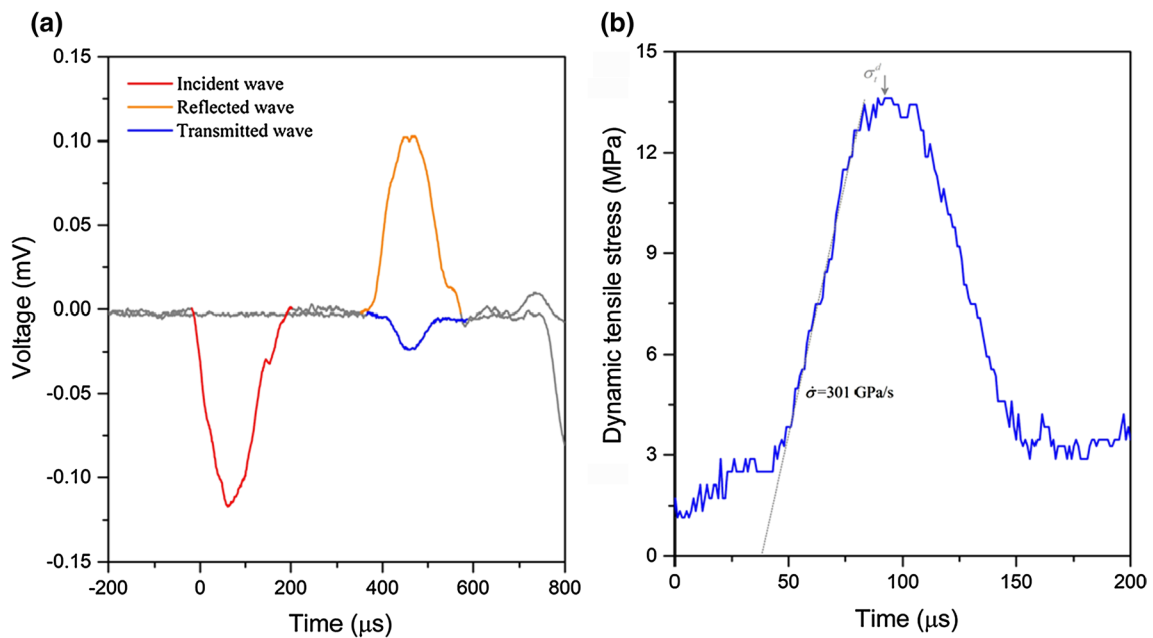


Fig. 6 a Raw data recorded in a typical dynamic BD test; b history curves of dynamic tensile stress

$$\begin{cases} F_1(t) = E_b A_b [\epsilon_I(t) + \epsilon_R(t)] \\ F_2(t) = E_b A_b \epsilon_T(t) \end{cases}, \quad (2)$$

where F_1 and F_2 are the dynamic forces during testing; E_b and A_b are the elastic modulus and the cross-sectional area of the bars; ϵ_I , ϵ_R and ϵ_T are the measured strain signals (see the original data in Fig. 6a) on the bars.

When the stress equilibrium on both ends of the sample is satisfied, i.e., $\epsilon_I(t) + \epsilon_R(t) = \epsilon_T(t)$, the average dynamic force (\bar{F}) is

$$\bar{F}(t) = \frac{1}{2} E_b A_b [\epsilon_I(t) + \epsilon_R(t) + \epsilon_T(t)] = \frac{1}{2} E_b A_b \epsilon_T(t). \quad (3)$$

3.3 Testing method

We conduct Brazilian disc (BD) tests to determine the tensile strength (TS) of rock samples under both quasi-static and dynamic loading conditions. According to the principle of BD testing [6], the BD sample is diametrically compressed to induce tensile stresses normal to the vertical diameter. If the failure of the BD sample initiates at the disc center where the maximum tensile stress should theoretically locate, the TS (σ_t) under quasi-static condition can be calculated as [30]

$$\sigma_t = \frac{2F_{\max}}{\pi DB}, \quad (4)$$

where F_{\max} is the maximum load during the BD test; D and B are the diameter and thickness of the BD sample, respectively.

Theoretical and experimental studies indicate that in dynamic tests, the TS can be determined as the quasi-static form when the force equilibrium is reached [44]:

$$\sigma_t^d(t) = \frac{2\bar{F}(t)_{\max}}{\pi DB}, \quad (5)$$

where σ_t^d is the dynamic TS and $\bar{F}(t)_{\max}$ is the maximum value of the average dynamic force (\bar{F}) on both sides of the BD sample.

3.4 The determination of loading rate

A large number of previous studies indicate that the dynamic strength of rock materials is greatly sensitive to loading rate or strain rate under dynamic loading conditions [20, 45]. The dynamic TS of rock is comparable at similar rate levels. Figure 6b shows the evolution curves of the tensile stress and strain rate with time during a typical dynamic BD test. We can see that the curve of dynamic stress evolution displays a linear period from 50 to 75 μ s when the stress increases steadily with time. The loading rate of this sample is characterized by the slope of the linear regime [31].

In SHPB tests, the loading rate is controlled by the gas pressure actuating the striker launched from the gas gun. In this study, the dynamic loading rates of BD samples range from 100 to 600 GPa/s. For comparison, quasi-static BD tests are also conducted using a servo-controlled material testing machine (MTS-647) at a constant loading rate of 10^{-4} GPa/s.

4 Test results

4.1 Macroscopic failure pattern

Figure 7 shows the failure patterns of postmortem YN sandstone samples with different water contents. As shown in

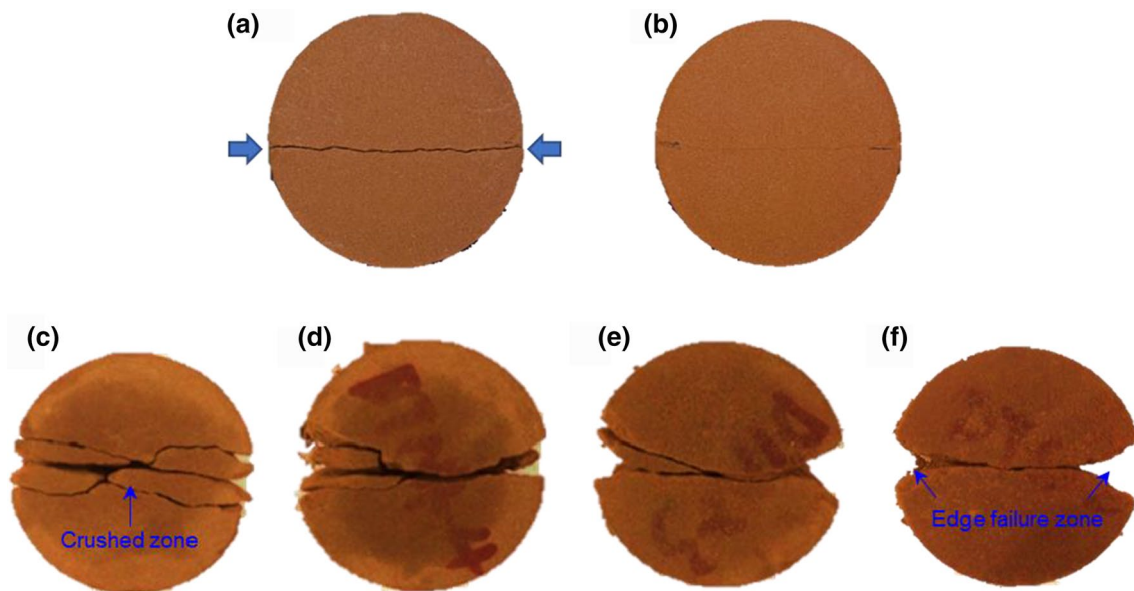


Fig. 7 Failure patterns of sandstone samples: **a** dry and **b** saturated samples under quasi-static loading condition; **c–f** samples with water contents of 0, 1, 2 and 3.5% under dynamic loading conditions at a loading rate of 200 GPa/s

Fig. 7a and b, in the quasi-static loading test, regardless of water content, the BD samples are split into perfect halves along the diametrical loading path. No observable damage occurs in the area contacting the loading platen. The failure patterns of the samples are, however, evidently affected by water content under dynamic loading condition (200 GPa/s), although all samples still seem to be split along the diametrical line. For the dry sample, there is sometimes more than one crack along the failure line, forming a crushed zone (see Fig. 7c). As the water content rises, the sample tends to fail with fractured zones near the loading points. The sandstone sample is softened greatly after being well saturated and deforms more easily under external force [2]. When subjected to dynamic loading, the zone near the loading point deforms very quickly, and the compressive and shear stresses between the sample and bars result in local damage. Thus, wedge-like damage zones occur at the edges of samples with relatively higher water contents during dynamic BD tests.

4.2 Dynamic failure process

The test result is valid only if the primary crack initiates at the center of the BD sample according to the assumptions of BD testing [6]. Therefore, the fracturing processes of samples were monitored and recorded by a high-speed camera to verify the validity of each test.

Figure 8a shows the fracture process of the dry sample in the dynamic BD test (corresponding to Fig. 7c). It can be clearly seen that a macrocrack first occurs at the center of the BD sample at 117 μ s. Then the central crack propagates along the loading direction until it totally coalesces at 169 μ s. After that, several secondary cracks develop to form a central crushing zone. This failure process is obedient to tensile fracturing. Equations 4 and 5 are valid for the calculation of tensile strength provided that the force equilibrium on both ends of the sample is met. For the water-saturated sample (Fig. 8b), although the final pattern (Fig. 7f) is such different from that of the dry sample, its test datum is still valid due to the primary crack initiating at the sample center followed by edge indentation.

4.3 Effect of water content on dynamic tensile strength of sandstone

After the check of crack initiation and force equilibrium, the dynamic TS of samples in valid tests was obtained as listed in Table 1. Figure 9 shows the relationship between the TS and water content for BD tests conducted under seven loading rates. We can see that the changing trends of TS against water content are dependent on loading rate. Under quasi-static loading condition, when the water content rises to 1.0% from 0, the TS of the YN sandstone displays a negligible reduction of 1.44%. After that, the TS remarkably

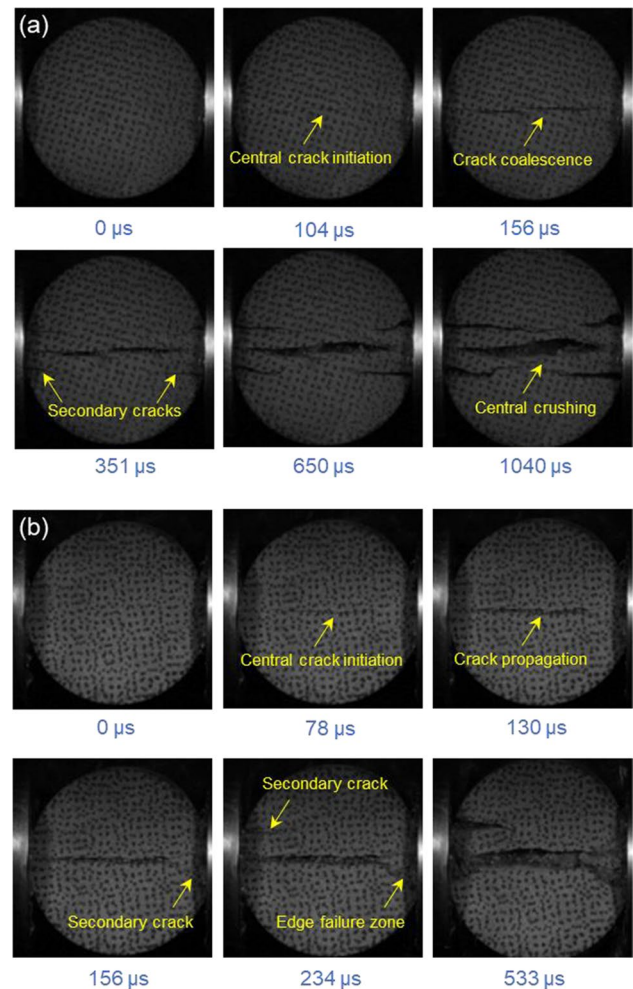


Fig. 8 Fracturing processes of **a** dry and **b** saturated samples obtained by a high-speed camera in typical dynamic BD tests

declines as water content increases (Fig. 9a). Similarly, at a loading rate of 100 GPa/s, the TS experiences a weakening pattern of “no change followed by a fast drop”. However, when the loading rate exceeds 200 GPa/s, the TS of the YN sandstone increases first and then decreases with increasing water content (Fig. 9c–g). The peak value of TS occurs at the water content of 1.0%. Taking the results at 500 GPa/s as an example (Fig. 9f), the average TS of dry samples is 13.4 MPa. When water content is 1.0%, the TS is 14.5 MPa, rose by 8.21%. After that, the TS gradually drops as the water content rises.

4.4 Rate dependence of tensile strength of sandstone samples

To further elucidate the relationship between the loading rate and the TS of samples with each water content, the tested data are plotted in terms of water content, as shown in Fig. 10. The dynamic TS of the YN sandstone samples is

Table 1 Test results of BD tests in this study

w/%	Designed $\dot{\sigma}$ /GPa	n	Actual $\dot{\sigma}$ /GPa/s		Tensile strength/MPa		DIF
			Ave	STD	Ave	STD	
0.0	10^{-4}	4	10^{-4}	0.00	1.7	0.05	–
	100	4	98	5.79	8.8	0.29	5.06
	200	4	205	6.13	10.6	0.34	6.14
	300	3	301	5.35	11.5	0.23	6.65
	400	4	388	5.95	12.8	0.40	7.37
	500	4	497	6.17	13.4	0.33	7.70
1.0	10^{-4}	4	10^{-4}	0.00	1.7	0.05	–
	100	4	102	7.45	8.7	0.56	5.07
	200	4	201	7.40	11.4	0.60	6.64
	300	4	289	6.51	12.5	0.60	7.30
	400	3	410	9.50	13.5	0.42	7.88
	500	3	492	7.46	14.5	0.42	8.46
2.0	10^{-4}	4	10^{-4}	0.00	1.4	0.06	–
	100	4	106	6.91	7.9	0.68	5.47
	200	2	203	6.89	10.1	0.90	6.98
	300	4	296	5.39	11.7	0.72	8.10
	400	3	397	8.97	12.5	0.85	8.67
	500	4	502	6.91	13.2	0.55	9.14
3.5	10^{-4}	4	10^{-4}	0.00	1.2	0.05	–
	100	3	102	4.14	7.0	0.31	5.75
	200	3	198	5.90	8.8	0.47	7.23
	300	4	304	5.89	10.7	0.53	8.82
	400	4	417	5.72	11.9	0.55	9.82
	500	3	508	6.09	12.6	0.57	10.44
	600	4	611	6.22	13.2	0.53	10.92

$\dot{\sigma}$ loading rate, n number of valid data, *Ave* average value, *STD* standard deviation, *DIF* dynamic increase factor

greatly sensitive to loading rate regardless of water content; in other words, the dynamic TS rises with increasing loading rate. Previous studies suggested that the dynamic strength of rock follows a positive power correlation with loading rate (or strain rate) as [46, 47]

$$\sigma_i^d(\dot{\sigma}) = a\dot{\sigma}^b, \quad (6)$$

where $\dot{\sigma}$ is loading rate; a and b are fitting constants. The constants a and b and the determination coefficients (R^2) obtained by Eq. 6 for samples with specific water contents are listed in Table 2. The high values of the determination coefficient and the good agreement between the test data and fitting curves (see Fig. 10) indicate that the power model can properly describe the $\sigma_i^d/\dot{\sigma}$ correlation.

Parameter b is a dimensionless constant characterizing the rising rate of strength with increasing loading rate (rate dependence). The higher the value of b is, the stronger the

dependence of the dynamic TS on the loading rate. From Fig. 11a, we can clearly observe that the value of b significantly rises with increasing water content. The dynamic increase factor (DIF, the ratio of dynamic strength to quasi-static strength) is another important indicator to characterize the loading rate effect on rock strength. Figure 11b further exhibits the DIF change in the TS of YN sandstone samples with different water contents. At given loading rates, the DIF of TS continuously rises with increasing water content. Another observation is that the sample with a higher water content has a greater increasing rate of DIF, resulting in the difference in DIF between the samples with various water contents growing much more evident as the loading rate increases. These findings suggest that the presence of water encourages rock strength to grow under dynamic loading circumstances. The underlying mechanisms will be discussed later.

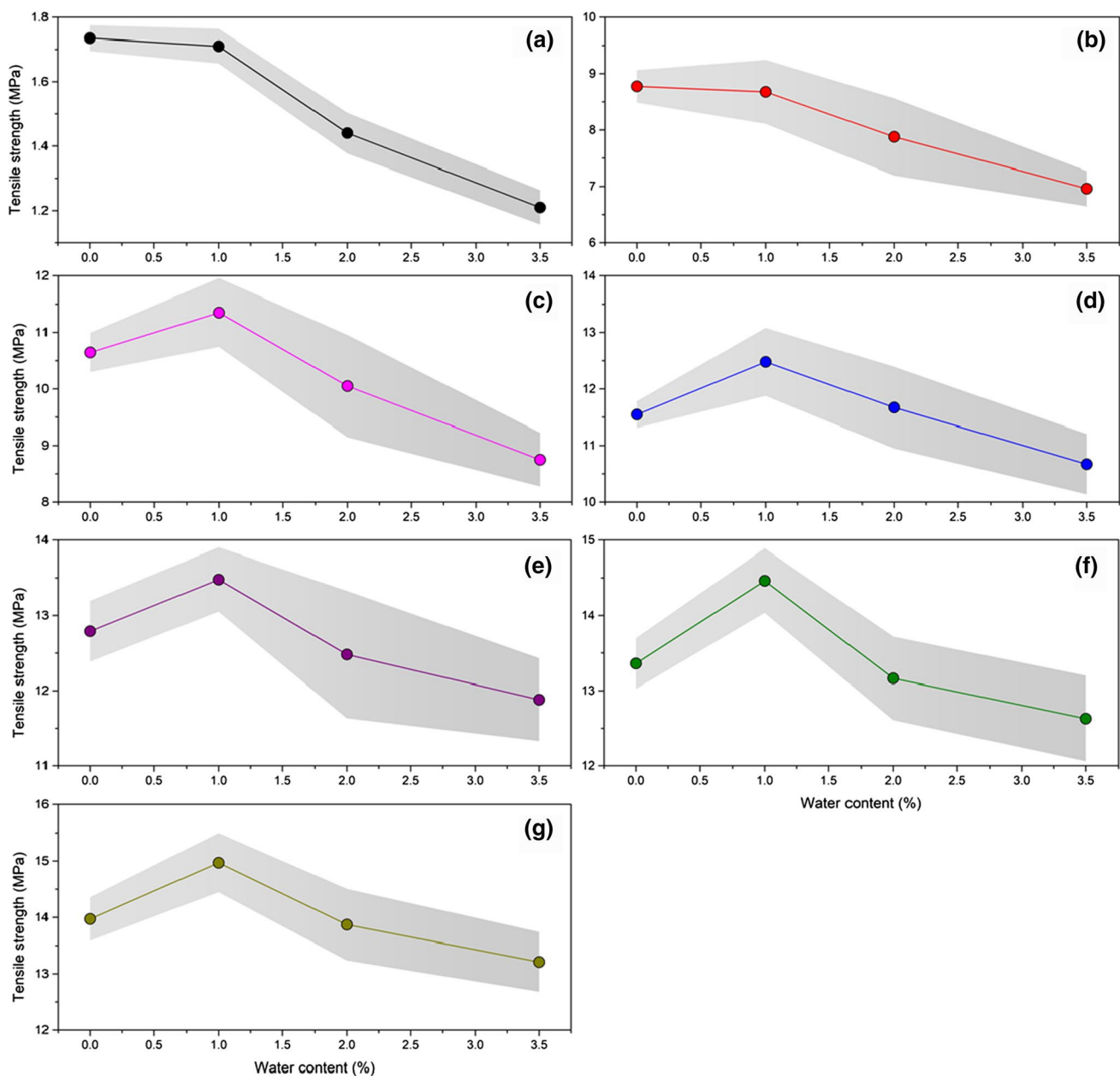


Fig. 9 Tensile strength of sandstone sample against water content at different loading rates: **a** 10^{-4} , **b** 100, **c** 200, **d** 300, **e** 400, **f** 500 and **g** 600 GPa/s

4.5 Water-affecting factor of tensile strength at different loading rates

The water-affecting factor (WAF), defined as the ratio of the strength of the wet sample to that of the dry sample obtained at the same loading rate, is applied to quantify the effect of water content on the tensile strength of YN sandstone. To diminish the deviation of the loading rate, the values of dynamic TS are not chosen from the actual tested data (Table 1) but are

calculated by fitting power functions (see Table 2) at loading rates of 100–600 GPa/s (with a constant interval of 100 GPa/s).

Figure 12 shows the WAF versus loading rate for the samples with different water contents. At a given loading rate, the WAF declines with increasing water content. Similar to TS, the WAF of the YN sandstone samples is also positively dependent on the loading rate. Additionally, the rising rate of the WAF against the loading rate rises

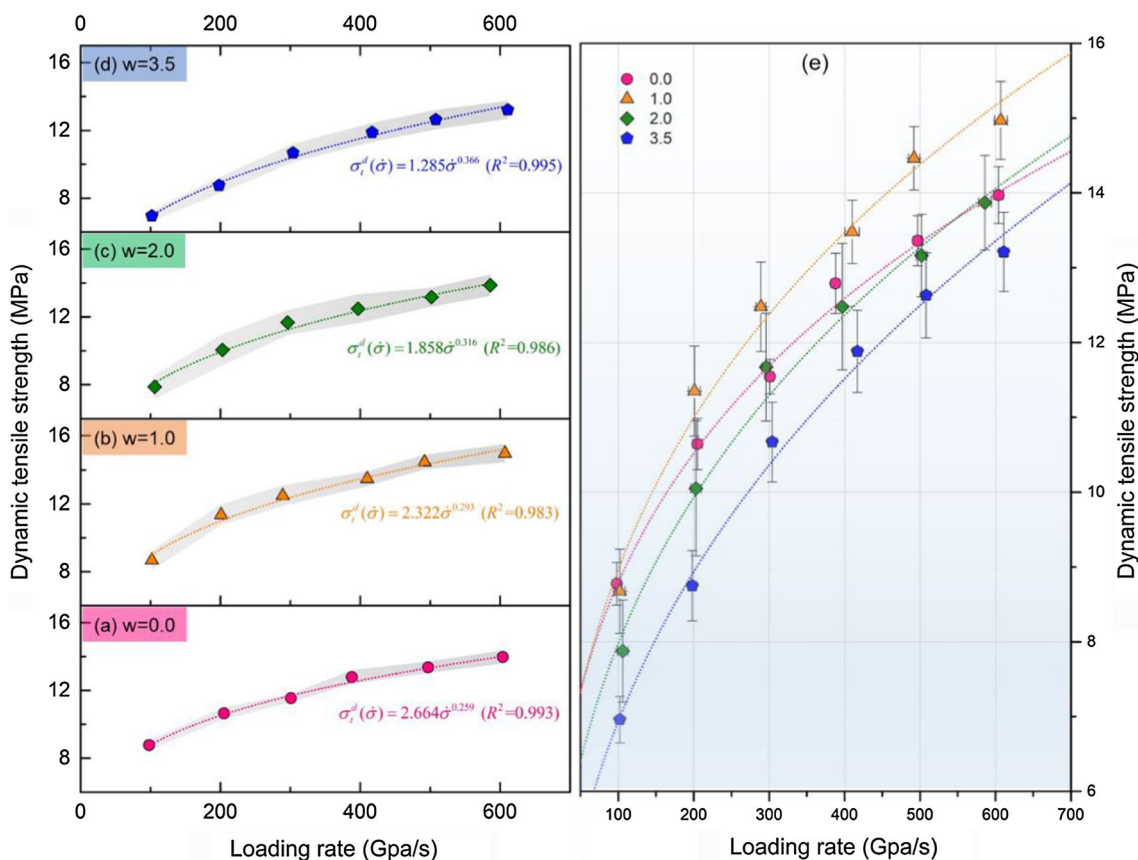


Fig. 10 Dynamic tensile strength of sandstone with water contents of **a** 0, **b** 1.0%, **c** 2.0%, and **d** 3.5% and **e** overview of the test results (scatters are average results in tests, lines are fitting curves obtained by Eq. 5)

Table 2 Correlations between loading rate and dynamic tensile strength under different water contents

w/%	Expression equation	a	b	R ²
0	$\sigma_t^d(\dot{\sigma}) = 2.664 \dot{\sigma}^{0.259}$	2.664	0.259	0.993
1.0	$\sigma_t^d(\dot{\sigma}) = 2.322 \dot{\sigma}^{0.293}$	2.322	0.293	0.983
2.0	$\sigma_t^d(\dot{\sigma}) = 1.858 \dot{\sigma}^{0.316}$	1.858	0.316	0.986
3.5	$\sigma_t^d(\dot{\sigma}) = 1.285 \dot{\sigma}^{0.366}$	1.285	0.366	0.995

with increasing water content. Therefore, the difference in the WAF caused by water content will be gradually diminished as the loading rate increases.

From Fig. 12, we can also observe that under quasi-static loading condition (10⁻⁴ GPa/s), the WAF values of all samples are lower than 1.0, which means that water weakens the quasi-static TS of the YN sandstone. Interestingly, the response of TS is affected by water content when subjected to dynamic loading. For samples with a water content of 1.0%, their WAFs are higher than 1.0 when the loading rate exceeds 100 GPa/s. This implies that the relatively lower water content plays an enhancing role in the tensile strength

under higher loading rate. However, when the water contents are 2.0% and 3.5%, the values of WAF are still lower than 1.0 but gradually approach unity with increasing loading rate.

5 Discussion

5.1 Water-weakening mechanisms under quasi-static loading condition

Various mechanisms have been proposed for water-weakening effects on rock strength, in which the pore pressure increase [47, 48], frictional reduction [49], and physical and chemical reactions [50, 51] are widely accepted. However, the dominant factor hinges on rock types and testing conditions [52]. For BD testing, the effects of pore pressure and frictional reduction are negligible due to tension-induced rock failure. According to the mineral composition of the YN sandstone (Fig. 3b), the water-weakening effects on the quasi-static TS are possibly attributed to physical and chemical reactions between rock/distilled water. Concretely speaking, quartz hydrolysis (also called stress corrosion)

Fig. 11 **a** Variation of b versus water content; **b** variation of DIF versus loading rate

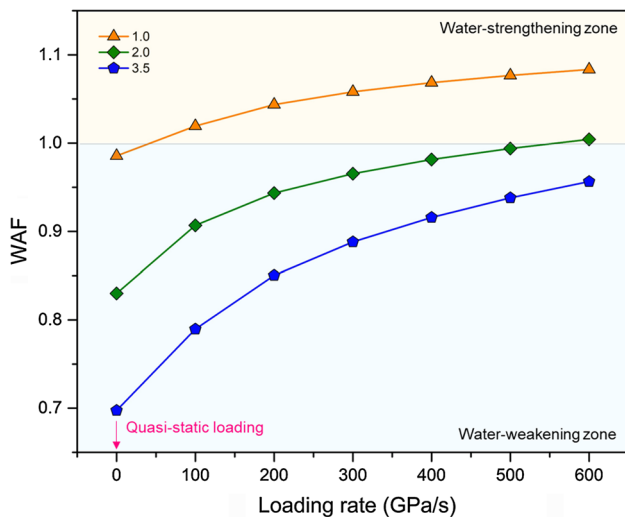
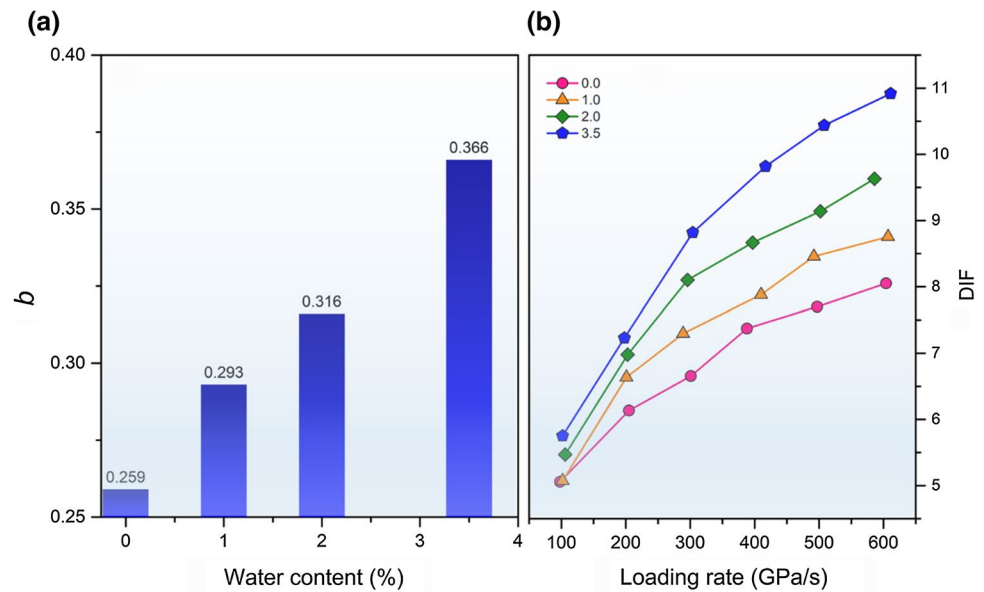


Fig. 12 WAF of tensile strength for YN sandstone with different water contents against loading rate

[51], clay softening and swelling [53] and calcite dissolution [50] can deteriorate the rock skeleton, which could be primarily responsible for TS loss.

There exists another interesting observation that the reduction in TS of the sample with 1.0% water content is absent under quasi-static loading condition (see Fig. 9a). The probable reasons are as follows: (1) the quartz hydrolysis is limited by the lower volume of water in pores, which causes the free water to hardly arrive at crack tips during loading; (2) the 30 min imbibition duration needed for the dry sample to obtain a 1.0% water content is not enough for the full reactions between minerals and water; and (3) only wetting the outside but the rock core still maintains a dry state. The last speculation can be verified by nuclear magnetic

resonance (NMR) images showing the water imbibition process (see Fig. 13). We can clearly observe that water molecules migrate from the free surface of the BD sample into its core during imbibition, and the dry state of the rock core with a 1.0% water content is not actually changed, which leads to the change in TS being insignificant when the water content is 1.0% as tensile cracks initiate at the center of the BD sample.

5.2 Strength compensation under dynamic loading condition

In dynamic BD tests, the rate dependence of TS rises with increasing water content (Fig. 10). The WAF also increases against loading rate. In particular, the WAF of the sample with a 1.0% water content is greater than 1.0. These phenomena indicate that water plays an enhancing role in rock strength under high loading rates. Previous studies suggested that the rate dependence of rock strength mainly contributes to the inertial effect and the viscous behavior of bulk materials in defects [20, 54]. Therefore, we can rationally speculate that water-enhancing effects under high loading rates involve the following mechanisms:

1. Increase in the inertia effect: when subjected to dynamic loading, the rock deforms very fast. The inertia of rock causes confinement (σ_r) to enhance its strength. The contribution magnitude of the inertial effect to rock strength is proportional to both rock density and loading rate [55].
2. Invalidation of quartz hydrolysis: quartz hydrolysis is only valid when water can diffuse into newly created crack tips instantly [51]. However, the crack speed of

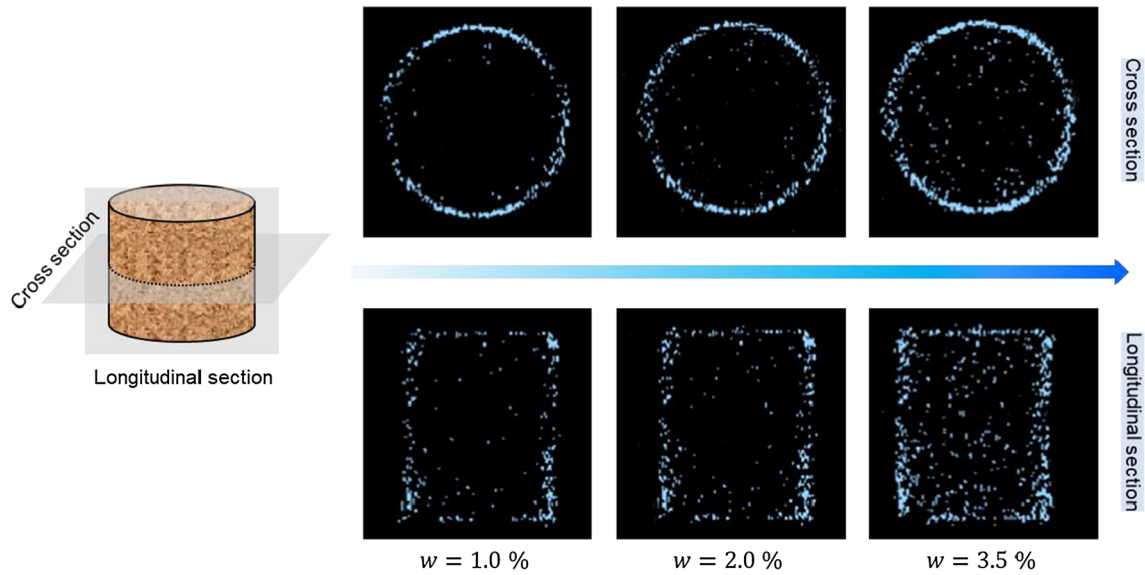
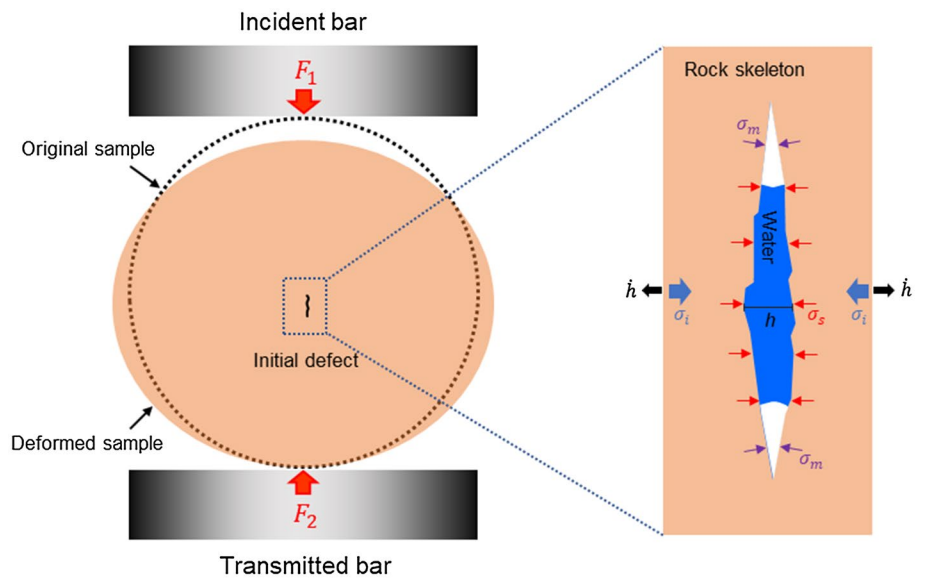


Fig. 13 NMR images for sections of the YN sandstone with different water contents (blue dots are molecules of free water)

Fig. 14 Schematic of stresses induced by free water at the central initial defect in the dynamic BD test



rock during dynamic loading is too high to allow water to spread to crack tips [45, 56], such that quartz hydrolysis is disabled.

3. Meniscus effect: under dynamic loading conditions, a roughly circular meniscus of water will be generated near the crack tip because the speed of water flow is much slower than the crack speed. The meniscus will exert suction stress (σ_m) on the walls of the crack tip to restrain crack propagation (see Fig. 14). The resisting stress induced by Meniscus effect is [57]:

$$\sigma_m = \frac{2V\gamma \cos \theta}{Ah^2}, \tag{7}$$

where V is the volume of free water; γ is the surface energy of water; θ is the wetting angle of the meniscus; h is the initial distance between the defect walls; A is the surface area of the defect wall. σ_m is proportional to the volume of free water in the defect but not dependent on the loading rate.

4. Stefan effect: in the case of a volume of water being trapped between two parallel plates with a small distance h , an opposing force can be deduced when the plates are separated with a high speed \dot{h} . The sidewalls of the defect can be considered as pairs of plates. When the BD sample is loaded dynamically, both sidewalls of the central defect are separated very fast, and free water can exert tensile stress on the walls to hinder crack opening

and propagation due to its viscosity (Fig. 14). The average stress caused by Stefan effect (σ_s) is expressed as [57]:

$$\sigma_s = \frac{3\eta V^2}{2\pi Ah^5} \cdot \dot{h}, \quad (8)$$

where η is the viscosity of the liquid; $\dot{h} = dh/dt$ is the relative speed of the two walls of the defect. σ_s is proportional to the loading rate as dh is proportional to the external force.

For simplification, we assume that under completely dry condition, the measured dynamic TS of rock without the consideration of micro- and macro-fracturing patterns can be expressed as

$$\sigma_t^d = \sigma_t^s + f(\sigma_i), \quad (9)$$

where σ_t^s is the quasi-static TS of the rock skeleton; $f(\sigma_i)$ is the strength enhancement by inertia. Following the same logic, due to the meniscus effect and Stefan effect, the dynamic TS of wet rock should be expressed as (Fig. 14)

$$\sigma_t^d = \sigma_t^{sw} + f(\sigma_i) + f(\sigma_m) + f(\sigma_s), \quad (10)$$

where σ_t^{sw} is the quasi-static tensile strength of the rock skeleton with a given water content; $f(\sigma_m)$ and $f(\sigma_s)$ are strength enhancements caused by the meniscus effect and Stefan effect, respectively.

The above simple models suggest that the strength of wet rock is governed by the coupled effects of water weakening and enhancement. Some experimental observations in this study can be interpreted by the dual effects of water:

1. Why does the sample with a higher water content have a greater rate dependence? Under dynamic loading, the enhancing effects of water are activated. At the same loading rates, $f(\sigma_i)$ increases with increasing water content on account of the higher density of rock samples with higher water content. Additionally, the terms $f(\sigma_m)$ and $f(\sigma_s)$ are always promoted by the volume of water in the defect according to Eqs. 7 and 8. Hence, the dynamic strength increment to the quasi-static strength is much more significant as the water content rises at a certain loading rate.
2. How does the water content affect the tensile strength of rock under dynamic loading? The rock strength is the result of competition between water weakening and enhancing effects. When experiments are conducted under quasi-static loading conditions, the presence of water plays an absolute weakening role due to the deac-

tivation of the enhancing effects at such slow loading rates. The effects of water are, however, much more complicated under dynamic loading conditions. For the sample with a water content of 1.0%, the water-enhancing effects control the rock strength due to the limited weakening effects, which leads to the dynamic TS exceeding the value of the dry sample. However, when the water content is greater than 2.0%, the TS of rock is still lower than that of dry rock at relatively lower loading rates, but the WAF notably rises compared to that tested under quasi-static condition. This is likely because the strength reduction caused by water-weakening is partially compensated by the activated water-enhancing effects, although the weakening factors of water are still dominant. Owing to the greater rate dependency of the rock sample with higher water content, water-weakening effects will be totally offset by the enhancing effects provided that the loading rate is high enough. It is thus speculated that the dynamic TS of rock with a water content greater than 1.0% will ultimately surpass that of dry rock as the loading rate increases. For the water content of 2.0%, the critical loading rate is 500 GPa/s, which further lends credence to our deduction. Unexpectedly, the dynamic TS of water-saturated samples (3.5%) is always lower than that of dry samples for the explored loading rate range. This could be ascribed to the fact that (1) the loading rate is still not high enough. The strength of the saturated sample likely exceeds that of the dry sample if the loading rate progressively rises according to the TS increasing trends against the loading rate; (2) the opposing force induced by the Stefan effect is limited by the adhesion between the wall of the rock defect and water [58]. Further work is needed to verify the explanation.

6 Conclusions

In this paper, dynamic Brazilian disc tests were performed on sandstone samples with water contents of 0, 1.0, 2.0 and 3.5% under various loading rates (up to 600 GPa/s) using an SHPB setup. The effects of water content on the tensile strength (TS) and its rate dependence of YN sandstone under dynamic loading conditions were investigated. Main conclusions can be drawn as follows:

1. The variation trends of TS in terms of water content are controlled by the loading rate. At a relatively lower loading rate (less than 100 GPa/s), the trend of TS displays the “no change followed by fast drop” pattern with increasing water content. However, the TS changes in the manner of an “initial rise followed by a gradual reduction” once

the loading rate exceeds 200 GPa/s, in which the turning point of the water content is between 1.0 and 2.0%.

2. For any water content, the TS of the YN sandstone increases with increasing loading rate. The rate dependence of TS is stronger in the sample with a higher water content.
3. Two types of competitive mechanisms codetermine the dynamic TS of wet rocks. On the one hand, water-weakening effects deteriorate the skeleton of rock, which are responsible for TS reduction. On the other hand, water-enhancing mechanisms, including increasing inertia effect, the invalidation of quartz hydrolysis, Meniscus and Stefan effects, are activated at high loading rates. All of these favor the increase of TS. The water-enhancing effects of rock are proportional to both the water content and loading rate.
4. Limitations and prospects: the water-enhancing effects on rock strength are qualitatively analyzed and discussed in the present study. However, the quantitative contributions of the specific water-enhancing effect to rock strength at different loading rates are still not unknown due to the difficult determination of several parameters in Eqs. 7 and 8. More elaborate experiments should be designed and conducted to validate these speculations, such as the influences of fluid viscosity, porosity and pore geometry on the resisting stress caused by Meniscus and Stefan effects under dynamic loading conditions. Moreover, in terms of numerical modeling, it is very promising that the functions for water-induced resisting forces are imbedded into a numerical code to explore the dynamic behavior of wet rocks.

Acknowledgements The work is supported by financial grants from the National Natural Science Foundation for Young Scientists of China (52104111), the National Natural Science Foundation of China (41772313) and the Natural Science Foundation of Hunan (2021JJ30819, 2015JJ4067). The authors are very grateful to the financial contribution and convey their appreciation for supporting this basic research.

Author contributions XC: conceptualization, methodology, testing, and writing. CC: sample preparation, data processing, and visualization. YZ: writing—review and editing. ZZ: supervision and writing—review and editing. SW: revision.

Declarations

Conflict of interest The authors declare that they have no known competing financial interests or personal relationships that could have appeared to influence the work reported in this paper.

References

1. Cai X, Cheng C, Zhou Z, Konietzky H, Song Z, Wang S. Rock mass watering for rock-burst prevention: some thoughts on the mechanisms deduced from laboratory results. *Bull Eng Geol Environ*. 2021. <https://doi.org/10.1007/s10064-021-02467-0>.
2. Wong LNY, Maruvanchery V, Liu G. Water effects on rock strength and stiffness degradation. *Acta Geotech*. 2016;11:713–37. <https://doi.org/10.1007/s11440-015-0407-7>.
3. Iverson RM. Landslide triggering by rain infiltration. *Water Resour Res*. 2000;36:1897. <https://doi.org/10.1029/2000WR900090>.
4. Ma D, Kong S, Li Z, Zhang Q, Wang Z, Zhou Z. Effect of wetting-drying cycle on hydraulic and mechanical properties of cemented paste backfill of the recycled solid wastes. *Chemosphere*. 2021. <https://doi.org/10.1016/j.chemosphere.2021.131163>.
5. Chugh YP, Missavage RA. Effects of moisture on strata control in coal mines. *Eng Geol*. 1981;17:241–55. [https://doi.org/10.1016/0013-7952\(81\)90001-6](https://doi.org/10.1016/0013-7952(81)90001-6).
6. Li D, Wong LNY. The Brazilian disc test for rock mechanics applications: review and new insights. *Rock Mech Rock Eng*. 2013. <https://doi.org/10.1007/s00603-012-0257-7>.
7. Tan L, Ren T, Dou L, Yang X, Qiao M, Peng H. Analytical stress solution and mechanical properties for rock mass containing a hole with complex shape. *Theor Appl Fract Mech*. 2021;114:103002. <https://doi.org/10.1016/j.tafmec.2021.103002>.
8. Hashiba K, Fukui K. Effect of water on the deformation and failure of rock in uniaxial tension. *Rock Mech Rock Eng*. 2015. <https://doi.org/10.1007/s00603-014-0674-x>.
9. Wong LNY, Jong MC. Water saturation effects on the Brazilian tensile strength of gypsum and assessment of cracking processes using high-speed video. *Rock Mech Rock Eng*. 2014;47:1103–15. <https://doi.org/10.1007/s00603-013-0436-1>.
10. Vutukuri VS. The effect of liquids on the tensile strength of limestone. *Int J Rock Mech Min Sci Geomech Abstr*. 1974;11:27–9. [https://doi.org/10.1016/0148-9062\(74\)92202-5](https://doi.org/10.1016/0148-9062(74)92202-5).
11. You M, Chen X, Su C. Brazilian splitting strengths of discs and rings of rocks in dry and saturated conditions. *Yanshilixue Yu Gongcheng Xuebao/Chin J Rock Mech Eng*. 2011;30:464–72.
12. Erguler ZA, Ulusay R. Water-induced variations in mechanical properties of clay-bearing rocks. *Int J Rock Mech Min Sci*. 2009;46:355–70. <https://doi.org/10.1016/j.ijrmms.2008.07.002>.
13. Ojo O, Brook N. The effect of moisture on some mechanical properties of rock. *Min Sci Technol*. 1990. [https://doi.org/10.1016/0167-9031\(90\)90158-O](https://doi.org/10.1016/0167-9031(90)90158-O).
14. Zhao Z, Yang J, Zhang D, Peng H. Effects of wetting and cyclic wetting-drying on tensile strength of sandstone with a low clay mineral content. *Rock Mech Rock Eng*. 2017;50:485–91. <https://doi.org/10.1007/s00603-016-1087-9>.
15. Yan Y, Liao Y, Wu J, Shi Y. Tension resistant strength of rock under confining pressure South China. *J Seismol*. 1991;11:1–12. <https://doi.org/10.13512/j.hndz.1991.02.001>.
16. Song Z, Konietzky H, Cai X. Modulus degradation of concrete exposed to compressive fatigue loading: Insights from lab testing. *Struct Eng Mech*. 2021;78:281–96. <https://doi.org/10.12989/sem.2021.78.3.281>.
17. Cheng R, Zhou Z, Chen W, Hao H. Effects of axial air deck on blast-induced ground vibration. *Rock Mech Rock Eng*. 2021. <https://doi.org/10.1007/s00603-021-02676-9>.
18. Song Z, Wang Y, Konietzky H, Cai X. Mechanical behavior of marble exposed to freeze-thaw-fatigue loading. *Int J Rock Mech Min Sci*. 2021. <https://doi.org/10.1016/j.ijrmms.2021.104648>.
19. Cai W, Dou L, Si G, Hu Y. Fault-induced coal burst mechanism under mining-induced static and dynamic stresses. *Engineering*. 2020. <https://doi.org/10.1016/j.eng.2020.03.017>.

20. Zhang QB, Zhao J. A review of dynamic experimental techniques and mechanical behaviour of rock materials. *Rock Mech Rock Eng.* 2014;47:1411–78. <https://doi.org/10.1007/s00603-013-0463-y>.
21. Li X. *Rock dynamics: fundamentals and applications*. Beijing: Science Press; 2014.
22. Huang S, Xia K, Yan F, Feng X. An experimental study of the rate dependence of tensile strength softening of Longyou sandstone. *Rock Mech Rock Eng.* 2010. <https://doi.org/10.1007/s00603-010-0083-8>.
23. Kim E, Changani H. Effect of water saturation and loading rate on the mechanical properties of Red and Buff Sandstones. *Int J Rock Mech Min Sci.* 2016. <https://doi.org/10.1016/j.ijrmmms.2016.07.005>.
24. Gombert P, Auvray C, Al-Heib M. In-situ and laboratory tests to evaluate the impact of water table fluctuations on stability of underground chalk mines. *Procedia Earth Planet Sci.* 2013. <https://doi.org/10.1016/j.proeps.2013.03.138>.
25. Zhou Z, Cai X, Ma D, Cao W, Chen L, Zhou J. Effects of water content on fracture and mechanical behavior of sandstone with a low clay mineral content. *Eng Fract Mech.* 2018. <https://doi.org/10.1016/j.engfracmech.2018.02.028>.
26. ASTM International, ASTM D2936-20, Standard Test Method for Direct Tensile Strength of Intact Rock Core Specimens, West Conshohocken, 2020. <https://doi.org/10.1520/D2936-20>.
27. ASTM International, ASTM D3967-16, Standard Test Method for Splitting Tensile Strength of Intact Rock Core Specimens, West Conshohocken, 2016. <https://doi.org/10.1520/D3967-16>.
28. Dai F, Xia K, Luo SN. Semicircular bend testing with split Hopkinson pressure bar for measuring dynamic tensile strength of brittle solids. *Rev Sci Instrum.* 2008. <https://doi.org/10.1063/1.3043420>.
29. Li X, Tao M, Wu C, Du K, Wu Q. Spalling strength of rock under different static pre-confining pressures. *Int J Impact Eng.* 2017. <https://doi.org/10.1016/j.ijimpeng.2016.10.001>.
30. ISRM. Suggested methods for determining tensile strength of rock materials part 2: suggested method for determining indirect tensile strength by the Brazil test. *Int J Rock Mech Min Sci Geomech Abstr.* 1978;15:99–103. [https://doi.org/10.1016/0148-9062\(78\)90003-7](https://doi.org/10.1016/0148-9062(78)90003-7).
31. Zhou YX, Xia K, Li XB, Li HB, Ma GW, Zhao J, Zhou ZL, Dai F. Suggested methods for determining the dynamic strength parameters and mode-I fracture toughness of rock materials. *Int J Rock Mech Min Sci.* 2012;49:105–12. <https://doi.org/10.1016/j.ijrmmms.2011.10.004>.
32. Zhou Z, Cai X, Cao W, Li X, Xiong C. Influence of water content on mechanical properties of rock in both saturation and drying processes. *Rock Mech Rock Eng.* 2016;49:3009–25. <https://doi.org/10.1007/s00603-016-0987-z>.
33. Xing HZ, Wu G, Dehkhoda S, Ranjith PG, Zhang QB. Fracture and mechanical characteristics of CO₂-saturated sandstone at extreme loading conditions. *Int J Rock Mech Min Sci.* 2019. <https://doi.org/10.1016/j.ijrmmms.2019.03.025>.
34. Liu Y, Dai F, Pei P. A wing-crack extension model for tensile response of saturated rocks under coupled static-dynamic loading. *Int J Rock Mech Min Sci.* 2021. <https://doi.org/10.1016/j.ijrmmms.2021.104893>.
35. Ogata Y, Jung W, Kubota S, Wada Y. Effect of the strain rate and water saturation for the dynamic tensile strength of rocks. *Mater Sci Forum.* 2004;465–466:361–6. <https://doi.org/10.4028/www.scientific.net/MSF.465-466.361>.
36. Cadoni E, Labibes K, Albertini C, Berra M, Giangrasso M. Strain-rate effect on the tensile behaviour of concrete at different relative humidity levels. *Mater Struct.* 2001;34:21–6. <https://doi.org/10.1007/BF02482196>.
37. Rossi P, Van Mier JGM, Toutlemonde F, Le Maou F, Boulay C. Effect of loading rate on the strength of concrete subjected to uniaxial tension. *Mater Struct.* 1994;27:260–4. <https://doi.org/10.1007/BF02473042>.
38. Zhao Y, Liu S, Jiang Y, Wang K, Huang Y. Dynamic tensile strength of coal under dry and saturated conditions. *Rock Mech Rock Eng.* 2016;49:1709–20. <https://doi.org/10.1007/s00603-015-0849-0>.
39. Petrov YV, Smirnov IV, Volkov GA, Abramian AK, Bragov AM, Verichev SN. Dynamic failure of dry and fully saturated limestone samples based on incubation time concept. *J Rock Mech Geotech Eng.* 2017;9:125–34. <https://doi.org/10.1016/j.jrmge.2016.09.004>.
40. Wang S, Tang Y, Wang S. Influence of brittleness and confining stress on rock cuttability based on rock indentation tests. *J Cent South Univ.* 2021. <https://doi.org/10.1007/s11771-021-4766-y>.
41. Li XB, Lok TS, Zhao J. Dynamic characteristics of granite subjected to intermediate loading rate. *Rock Mech Rock Eng.* 2005;38:21–39. <https://doi.org/10.1007/s00603-004-0030-7>.
42. Zhu Q, Ma C, Li X, Li D. Effect of filling on failure characteristics of diorite with double rectangular holes under coupled static-dynamic loads. *Rock Mech Rock Eng.* 2021. <https://doi.org/10.1007/s00603-021-02409-y>.
43. Han Z, Li D, Zhou T, Zhu Q, Ranjith PG. Experimental study of stress wave propagation and energy characteristics across rock specimens containing cemented mortar joint with various thicknesses. *Int J Rock Mech Min Sci.* 2020;131: 104352. <https://doi.org/10.1016/j.ijrmmms.2020.104352>.
44. Dai F, Huang S, Xia K, Tan Z. Some fundamental issues in dynamic compression and tension tests of rocks using split Hopkinson pressure bar. *Rock Mech Rock Eng.* 2010;43:657–66. <https://doi.org/10.1007/s00603-010-0091-8>.
45. Li XF, Li HB, Zhang GK, Ju MH, Zhao J. Rate dependency mechanism of crystalline rocks induced by impacts: insights from grain-scale fracturing and micro heterogeneity. *Int J Impact Eng.* 2021. <https://doi.org/10.1016/j.ijimpeng.2021.103855>.
46. Lankford J. Role of tensile microfracture in the strain rate dependence of compressive strength of fine-grained limestone—analogy with strong ceramics. *Int J Rock Mech Min Sci Geomech Abstr.* 1981;18:65. [https://doi.org/10.1016/0148-9062\(81\)91225-0](https://doi.org/10.1016/0148-9062(81)91225-0).
47. Cai X, Zhou Z, Zang H, Song Z. Water saturation effects on dynamic behavior and microstructure damage of sandstone: Phenomena and mechanisms. *Eng Geol.* 2020. <https://doi.org/10.1016/j.enggeo.2020.105760>.
48. Zhong C, Zhang Z, Ranjith PG, Lu Y, Choi X. The role of pore water plays in coal under uniaxial cyclic loading. *Eng Geol.* 2019;257: 105125. <https://doi.org/10.1016/j.enggeo.2019.05.002>.
49. Kawai K, Sakuma H, Katayama I, Tamura K. Frictional characteristics of single and polycrystalline muscovite and influence of fluid chemistry. *J Geophys Res Solid Earth.* 2015;120:6209–18. <https://doi.org/10.1002/2015JB012286>.
50. Ciantia MO, Castellanza R, di Prisco C. Experimental study on the water-induced weakening of calcarenites. *Rock Mech Rock Eng.* 2015;48:441–61. <https://doi.org/10.1007/s00603-014-0603-z>.
51. Atkinson BK, Meredith PG. Stress corrosion cracking of quartz: a note on the influence of chemical environment. *Tectonophysics.* 1981;77:T1–11. [https://doi.org/10.1016/0040-1951\(81\)90157-8](https://doi.org/10.1016/0040-1951(81)90157-8).
52. Van Eeckhout EM. The mechanisms of strength reduction due to moisture in coal mine shales. *Int J Rock Mech Min Sci Geomech.* 1976;13:61–7. [https://doi.org/10.1016/0148-9062\(76\)90705-1](https://doi.org/10.1016/0148-9062(76)90705-1).
53. Lyu Q, Ranjith PG, Long X, Kang Y, Huang M. A review of shale swelling by water adsorption. *J Nat Gas Sci Eng.* 2015;27:1421–31. <https://doi.org/10.1016/j.jngse.2015.10.004>.
54. Ožbolt J, Bošnjak J, Sola E. Dynamic fracture of concrete compact tension specimen: experimental and numerical study. *Int J Solids Struct.* 2013;50:4270–8. <https://doi.org/10.1016/j.ijsolstr.2013.08.030>.

55. Field JE, Walley SM, Proud WG, Goldrein HT, Siviour CR. Review of experimental techniques for high rate deformation and shock studies. *Int J Impact Eng.* 2004. <https://doi.org/10.1016/j.ijimpeng.2004.03.005>.
56. Zhou Z, Cai X, Ma D, Du X, Chen L, Wang H, Zang H. Water saturation effects on dynamic fracture behavior of sandstone. *Int J Rock Mech Min Sci.* 2019. <https://doi.org/10.1016/j.ijrmms.2018.12.014>.
57. Rossi P. A physical phenomenon which can explain the mechanical behaviour of concrete under high strain rates. *Mater Struct.* 1991;24:422–4. <https://doi.org/10.1007/BF02472015>.
58. Vegt I. *Concrete in dynamic tension: the fracture process*. Delft: Delft University of Technology; 2016.

Publisher's Note Springer Nature remains neutral with regard to jurisdictional claims in published maps and institutional affiliations.